18èmes Journées Internationales de Thermique (JITH 2017)
Monastir (Tunisie), 25 - 27 Octobre 2017

The energy performance of a façade solar heating system

Khelifa Hami[a,b] , Belkacem Draoui[b], Omar Imine[c], Omar Hami[b]
[a]*Institute of Sciences and the Technology, Tindouf University Center, BP: 407, 37000, Tindouf, Algeria*
[d]*Laboratory of energetic in the arid areas, ''ENERGARID'', University Tahri Mohammed, Bechar, Algeria*
[c]*Faculty of Mechanical Engineering, University of Sciences and Technology of Oran Mohamed BOUDIAF, USTO MB, BP: 1505, EL Mnaouar 31000, Oran, Algeria*
hamikhelifa@yahoo.fr
bdraoui@yahoo.com

Résumé : Natural convection phenomena have been and continue to be the subject of much research activities. However, we note that in the context of the habitat where the Rayleigh number is usually higher (10^{11} order), the experiments are rare and few calculations. So it is necessary first to make an effort to establish an accurate experimental device to explore and better understand the turbulent natural convection flows that develop in a residential part, and the other developing numerical tools that predict realistically the movement of air inside buildings. The natural convection in the system studied is fairly complex; it changes from the laminar flow to the turbulent flow and the turbulent flow covers at least half the height of massive wall during the normal circulation. In this work simulation in three-dimensional (3D) on the flow in a room coupled with a facade of passive heating system type: (In-In), were conducted numerically to determine all the thermals parameters, dynamics and turbulence's according to the climate conditions of the area studied.

Mots clés : Solar energy, Thermal models, Turbulence flows, Reynolds stress modeling.

1. Introduction

Considerable interest has been recently observed in passive solar heating systems, which combine the solar collection and thermal storage into the building structure and distribute the heat by natural methods. The Trombe wall is a kind of passive solar heating systems used for space heating.

The Trombe wall system consists of the south massive wall and a glass cover. Vents are located at both the top and the bottom of the wall. Solar heat, absorbed by the darkened massive wall surface, is transferred to the room by heat convection and conduction. Relatively cool air in the room, drawn through the bottom vents, is heated up as it passes thought the channel and then delivered into the room through the top vents by stack-effect. The thermo-circulation provides a direct heat path to the room, while the conduction through the wall has a time delay. These two paths are interactive.

Research on applications of solar heat in the home has been conducted on various devices, including prominently passive heating systems, which are quite relevant to the problem of thermal insulation from outside influences. [1] Passive heating systems are sensors that collect and store solar energy and contribute to thermal comfort in the building. The numerical approach is the use of the Navier–Stokes equations under certain simplifying assumptions to determine the air flow rate in this system. The mass conservation equations, speed, and energy are also used. Two numerical approaches have been used since the first numerical models of the 1960s. The first, used by Aung et al. [2] and Kaiser et al., [3] uses the Boussinesq approximation by considering all the constant physical parameters, except for the bulk density.

The rewriting of the Navier–Stokes equations then provides a problem, whose solutions can be calculated numerically relatively simply. The second considers the Navier–Stokes equations with non-constant parameters, such as those of Kaiser et al. [3] and Gan [4-5] This method is made possible by the development of computational tools and computational fluid dynamics (CFD) solving techniques. Several researchers have conducted studies on the numerical TROMBE wall and have developed models, which recognized the special nature of TROMBE walls with asymmetric heating channels and heat loss taking place through the glass, Burek et al. [6] and Ong [7] has developed a simplified thermal model based on the properties of the channel thickness and the thermal flux. Other thermal networks and simplified models have been developed to predict the

performance of the daytime solar chimney or TROMBE wall, especially Balocco[8]. Gan [4] for his part studied the movement of air in a ventilated room naturally through the use of a solar chimney or TROMBE wall for cooling buildings in summer.

Bouchair [9] showed that there is an optimal chimney length/width difference of maximum airflow. If the stack is too large, there is a reverse flow of air, thus an air flow down through the center of the conduit.

Bansal et al.[10] developed the mathematical model to predict the velocity of the air in a solar chimney from the prediction of the temperature of the absorbed, the air in the flow channel, and the glass plate. Experimental validation of the model was done using a solar chimney having an absorbed of 1 m height. The work carried out with three different combinations of air space and the air inlet in the fireplace dimensions showed good agreement between observed results and those calculated. The small size of the solar chimney analyzed opened opportunities to use the windows like solar chimneys, from flow velocities of more than 0.24 m/s. In Aung et al. [2] the term motor is considered to the temperature difference between the surface temperature of the plates and the temperature of the outside air or the heat flux at the plate interface between the solid and air.

The Grashof number is then defined accordingly. Similarly, CFD studies consider the boundary conditions of the air gap fixed temperatures, as do Chami and Zoughaib [11] or flow, as in Hami et al. [12] Then, the Nusselt number and the speed are calculated for different numbers of Rayleigh and aspect ratios. Correlations, to the convection coefficient and the average air speed, are then offered. Aung et al. [2] perform a number of calculations for Rayleigh numbers and selected flow rates. They then find an asymptotic relationship between Rayleigh number and Reynolds number and Rayleigh number on one hand and Nusselt number on the other.

Zamora and Kaiser [13] studied the flow (laminar and turbulent) in a solar chimney for different Rayleigh numbers and different aspect ratios, using a numerical code. Correlations giving the aspect ratio value, which maximizes the Nusselt number for the Rayleigh number values between 105 and 1012, were prepared. The more the number of Rayleigh is raised, the more the report of the shape must be low to maximize the convective exchanges. The maximum speed is reached for the maximum value of the Nusselt, which is explained by the fact that turbulent flow reversals take place, favoring the convective exchanges, but not the air exchange.

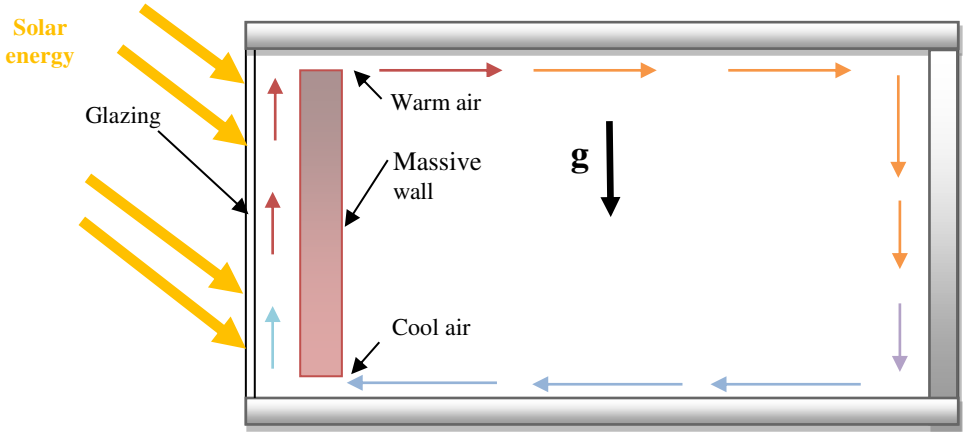

Figure 1: Physical model studies.

Gan [14] and Hami et al.[15] studied the solar chimneys, and provide general expressions for calculating first the Nusselt number as a function of the aspect ratio and the Rayleigh number, and second the Reynolds number based on the Rayleigh and Nusselt numbers, thereby obtaining the flow rate. It breaks these relations on the basis on which they are valid. Note that these relations are valid for flow from 100 to 1000 $W/m^2$and, for various distributions of flow between the two faces of the cavity. These methods have the advantage of a fine description of any flaw in the air space; they also help to analyze the nature of the flow locally including its potential heterogeneity along the canal. But these results are established for specific configurations and inputs, thereby limiting their use for modelling of exchanges in real configurations facade passive heating system coupled with the building.

In this work, three-dimensional (3D) simulations on the flow in a room coupled with a facade of passive heating system type: In-In (Trombe wall), Fig. 1. was conducted numerically to determine the temperature and velocity fields in the influence of the variation of the modified Rayleigh number, which itself depends on the characteristics of the fluid and heat flow due to the sunshine. The behavior of boundary layers in natural convection is analyzed along the Trombe wall in our periodically heated imposed flow. Thermal and dynamic modelling of the problem was made by CFD calculation, based on the finite volume method to model both the fluid flow and heat transfer. To take account of the strong temperature gradient and velocity near the walls, we

chose a structured tight mesh near the walls and a little wider mesh elsewhere. The results have shown that for $Gr_h < 4x10^8$, the flow regime is laminar, while for $Gr_h > 10^9$, the flow regime becomes turbulent.

2. Simulation Procedures

2.1. Mathematical model

2.1.1. Simplifying hypotheses

In order to obtain a mathematical model for the physical phenomenon studied, we adopt the following assumptions:

- The fluid is Newtonian and incompressible
- The flow regime is unsteady,
- The flow is generated transitional between laminar / turbulent along the Trombe Wall (hot wall),

The physical properties of the fluid are constant except the density obeys the Boussinesq approximation in terms of the buoyancy.

2.1.2. Equations of the problem

The equations governing the problem addressed are those turbulent incompressible flows and written decaying Reynolds for pressure, speed and temperature with an average component and a fluctuation term (1):

$$\begin{cases} P = \overline{P} + P' \\ u = \overline{u} + u' \\ T = \overline{T} + T' \end{cases} \quad (1)$$

And expressing respectively the mass conservation, momentum and energy:

$$\frac{\partial \overline{u}}{\partial x_i} = 0 \quad (2)$$

$$\frac{\partial \overline{u}}{\partial t} + \overline{u}_j \cdot \frac{\partial \overline{u_i}}{\partial x_j} = -\frac{1}{\rho} \cdot \frac{\partial \overline{P}}{\partial x_i} + \frac{\partial}{\partial x_j}\left[\nu \cdot \left(\frac{\partial \overline{u_i}}{\partial x_j} + \frac{\partial \overline{u_j}}{\partial x_i} \right) - \overline{u_i' u_j'} \right] + \overline{f_i} \qquad i = 1, 2, 3 \quad (3)$$

$$\frac{\partial \overline{T}}{\partial t} + \overline{u}_i \cdot \frac{\partial \overline{T}}{\partial x_i} = \frac{\partial}{\partial x_i}\left[\alpha \cdot \frac{\partial \overline{T}}{\partial x_i} - \overline{u_i T'} \right] \quad (4)$$

The Reynolds stresses and heat turbulent flows respectively appear in the equations (3) and (4) are expressed in terms of dynamic and thermal fields means as follows [17] :

$$\overline{u_i' u_j'} = \frac{2}{3} \cdot \delta_{ij} \cdot k - \nu_t \cdot \left(\frac{\partial \overline{u}_i}{\partial x_j} + \frac{\partial \overline{u_j}}{\partial x_i} \right) \quad (5)$$

$$\overline{u_i T'} = \frac{\nu_t}{\mathrm{Pr}_t} \cdot \frac{\partial \overline{T}}{\partial x_j} \quad (6)$$

Where: $\nu_t(x_i, t)$ is a turbulent kinematic viscosity.

$$\nu_t = C_\mu \cdot \frac{k^2}{\varepsilon} \quad (7)$$

$$\mathrm{Pr}_t = \frac{\nu_t}{\alpha_t} \approx 0.85 \text{ (for air) [17]} \quad (8)$$

To close the whole transport equations (2), (3) and (4), the turbulence model k-ε, (9) and (10) was used. This model has the advantage of not requiring very large computation times, especially for simple cases such as the one we are studying.

We will therefore use this model of turbulence with improved treatment laws, walls (Enhanced wall treatment), with the intention to resolve the laminar sub-layer, it is important to have the order y + (y + ~ 1). However, a larger value is acceptable as long as it remains in the viscous sub-layer (y + < 4 or 5) [22].
The two modelled equations of turbulent kinetic energy k, and ε dissipation are described by the following transport equations (9) and (10): [17-18].

2.1.2. Equation of turbulent kinetic energy

$$\frac{\partial k}{\partial t}+\bar{u}_j\frac{\partial k}{\partial x_j}=\frac{\partial}{\partial x_j}\left[\left(\nu+\frac{C_\mu\cdot k^2}{\sigma_k\varepsilon}\right)\frac{\partial k}{\partial x_j}\right]+\frac{C_\mu\cdot k^2}{\sigma_k}\left(\frac{\partial \bar{u}_i}{\partial x_j}+\frac{\partial \bar{u}_j}{\partial x_i}\right)\frac{\partial \bar{u}_i}{\partial x_j}-\varepsilon \qquad (9)$$

2.1.3. Equation of dissipation

$$\frac{\partial \varepsilon}{\partial t}+\bar{u}_j\frac{\partial \varepsilon}{\partial x_j}=\frac{\partial}{\partial x_j}\left[\left(\nu+\frac{C_\mu\cdot k^2}{\sigma_\varepsilon\varepsilon}\right)\frac{\partial \varepsilon}{\partial x_j}\right]+C_{\varepsilon 1}\cdot C_\mu\cdot k\cdot\left(\frac{\partial \bar{u}_i}{\partial x_j}+\frac{\partial \bar{u}_j}{\partial x_i}\right)\frac{\partial \bar{u}_i}{\partial x_j}-C_{\varepsilon 2}\cdot\frac{\varepsilon^2}{k} \qquad (10)$$

The constants called k-ε model are standards for values: [19]

$C_\mu=0.09$, $\sigma_k=1$, $\sigma_\varepsilon=1.22$, $C_{\varepsilon 1}=1.44$ $C_{\varepsilon 2}=1.9$

Transport equations (2), (3), (4), (9) and (10) are resolved by the method of the control volumes and resolved by the simple algorithm Patankar [19]. In order to achieve a compromise between the computation time and accuracy of simulation results, an optimization study was made of the influence of no space and time (Courant-Friedrichs-Lewy (1928) or CFL condition. It is necessary and sufficient for stability) [20]. It is estimated that convergence is reached when the relative differences in all variables calculated at various nodes of the mesh, fall below ($R = 10^{-4}$) between two successive iterations.

2.2. Initial and boundary conditions

At : t = 0, $u=v=w=k=\varepsilon=0$

$T=T_i=6°C$

- Condition of adherence to the walls (u, v, w) = (0,0,0);
- The contest between the Trombe wall (w) and air (f) is assumed to be perfect in the air space;

So : $x=\delta$ and $h_i\le y\le h_o$, $\quad -\lambda_w\frac{\partial T_w}{\partial y}=-\lambda_f\frac{\partial T_f}{\partial y}=\varphi_s$

$$T_w(y)=T_f(y)\ \text{(interface)}$$

- The estimated global solar radiation is expressed by the model of LUI&JORDAN [21]

$$\begin{cases}\varphi_s=S^*+D_i^* \ ; i=90° \text{ (for a vertical plan)}\\ S^*=I^*\times\left[\sin(i)\times\cos(h)\times\cos(a-\gamma)+\cos(i)-\sin(h)\right]\\ D_i^*=\left[\frac{1+\cos(i)}{2}\right]\times D_h^*+\left[\frac{1-\cos(i)}{2}\right]\times a^*\times G_h^*\\ D_h^*=G_h^*-I^*\times\sin(h)\end{cases}$$

- **Geophysics of the city of Bechar**: area selected in this work.
  - Latitude : 31 ° 62' N
  - Longitude : 2 ° 23' W
  - Altitude : 773m
  - Albedo : 0.2

- To : $x = L$ and $y = H$ $T = T_c$ (cold wall) ;
- Other surfaces are adiabatic : $\frac{\partial T}{\partial n} = 0$
- For the k-ε model, the equation of the turbulent kinetic energy k is solved in the whole field with a condition imposed on the walls is : $\frac{\partial k}{\partial n} = 0$, n : is the normal local coordinate to the wall.

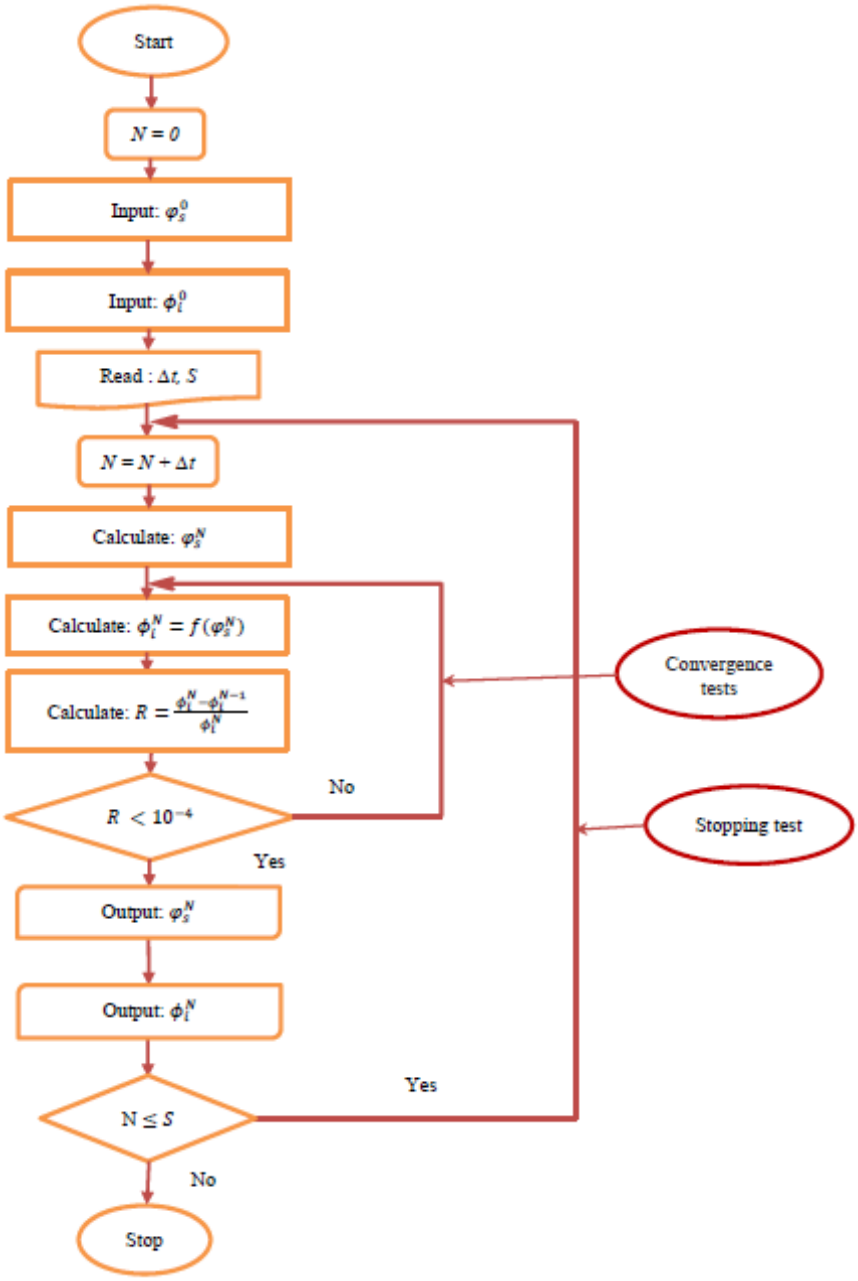

Figure 2: Flowchart of simulation process.

3. Results and discussion

All the thermals parameters, dynamics and turbulence's are calculated according to the climate conditions of the area studied. The natural convection in the channel is fairly complex; it changes from the laminar flow to the turbulent flow and the turbulent flow covers at least half the height of massive wall during the normal circulation

3.1. Validation of results

The problem of natural convection driven buoyancy in front of passive heating systems coupled with the building has been widely used by researchers in the field of heat the building as a test case for the validation of calculation methods [23 -24]. This same problem is here used to test this method. The results of this method for the number of local Grashof Gr_h depending on the height h relative to ref. [23-24] are shown in Figure 3.

Gr_h is defined by the following equation (11):

$$Gr_h = \frac{g \cdot \beta \cdot q_w \cdot h^4}{\nu^2 \cdot \lambda} \qquad (11)$$

Tableau 1: Nusselt for different correlations of the Ref. [23-24]

	Nulsset							
Gr_h	10^7		10^8		10^9		10^{10}	
		Error (%)		Error (%)		Error (%)		Error (%)
Present work	24.91	//	53.26	//	113.86	//	243.42	//
ARHARAE	23.90	4.23	51.07	4.29	109.19	4.28	233.45	4.27
Cibs	24.30	2.51	51.95	2.52	111.10	2.48	237.44	2.52
Ferris	25.32	1.62	54.13	1.61	115.72	1.61	247.41	1.61

Table 1 shows the values of average Nusselt according to local Grashof, these results are in good agreement in general, the values obtained by Ferris [23-24] are the closest to the results of this work.

The error are expressed as: $\text{Error} = \left| \frac{Nu_{\exp} - Nu_{prresent\_work}}{Nu_{\exp}} \right| (\%)$ (12)

Figure 3. illustrates in good general agreement is found between experiment Ref. [23-24] and simulations of this work, but with a small difference between the maximum and minimum Nulsset according to local Grashof.

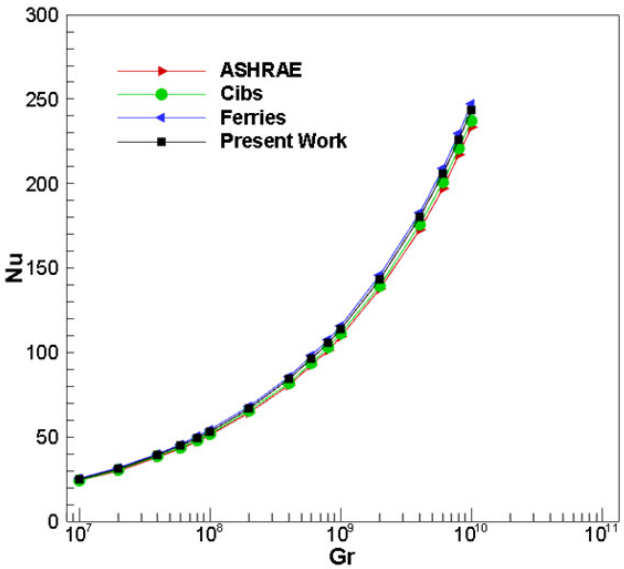

Figure 3:Validation of simulation results with ref. [24-25] according Grashof means Nulsset.

3.2. Independence of the mesh

It appears according to the face Fig. 4. And Figure 5., that the obtained solution is independent from the meshing because we notice the existence of a low difference in the evolution of the velocity in the vertical plane in the

middle of the premises on one hand, and on the other hand the values of the number of *Nulsset* on the hot and, cold wall. We note however, that the grid M3 gives slightly more important values with regard to comparing with two others (M1, M2). In the simulations which follow, we should use exclusively the grid M3.

Tableau 1: Meshes used for the simulation.

Cases	Size	Type	1st Mesh
M1	41616 cells	structured	0.004
M2	62592 cells	//	0.002
M3	104556 cells	//	0.001

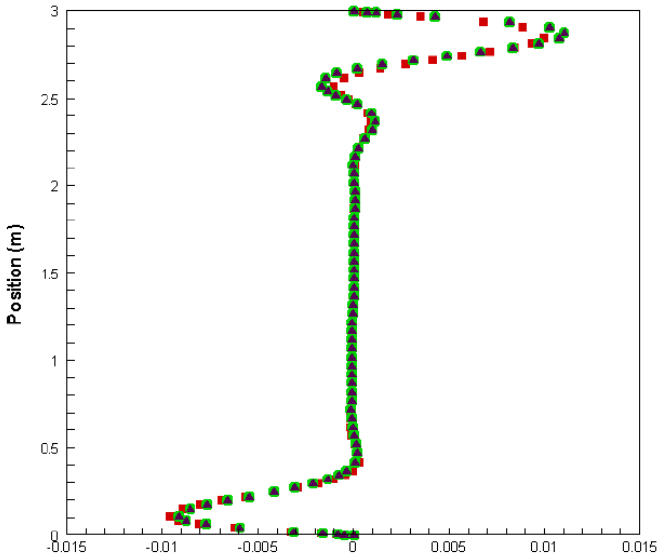

Figure 4:Velocity U in the middle of the local.

Figure 4 Represents the evolution of the speed you along the height in the middle of the room, we notice that there are three parts, the first is at the top (blowing zone hot air), the second is down (suction area of the cold air) and the third thermal laminating zone under the effect of volume forces, note here that in this area the speeds are negligible.

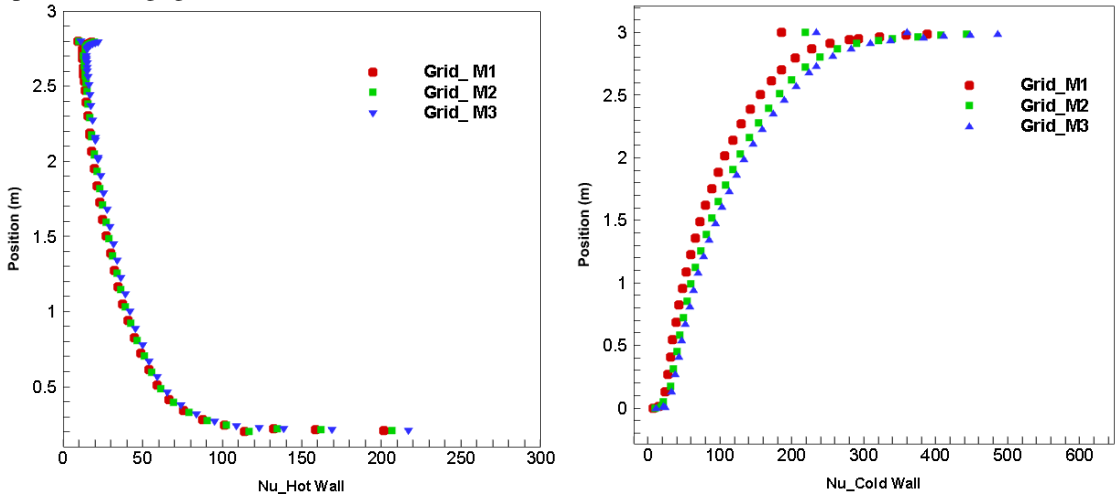

Figure 5: Nullset on the hot and cold wall.

3.3. Flow classification

Virtually the pressure is rendered no dimensional. As it depends on the flow velocity, it is presented in the form of a pressure coefficient C_p noted given by:

$$C_P = \frac{P - P_{ref}}{\frac{1}{2}\rho U_{ref}^2} \quad (13)$$

The pressure coefficient is relatively independent parameter of the flow velocity; it is related only to the geometry of the structure Fig. 6(b).

The action of the pressure does not represent all of the effort exerted by the air locally on the surface of the wall. In fact, air flow produces a boundary layer characterized by a velocity gradient in the wall. This gradient is the assumption of a linear Newtonian fluid with shearing stresses that result. This therefore adds to the pressure force, normal to the wall, a friction terms tangential due to the viscosity of air Fig. 6(a). This defines the coefficient of frictionC_f:

$$C_f = \frac{\tau_w}{\frac{1}{2}\rho U_{ref}^2} \quad (14)$$

Where$\tau_w$is the tangential stress at the wall.

Practically for our case the structure of the flow is not the fat profileto the presence of openings in the passive heating system studied, so that friction term is negligible compared with the action of pressure. The magnitude of the friction coefficient is 10^{-4}, compared to 10^{-2} for pressure coefficients (Fig. 6.).

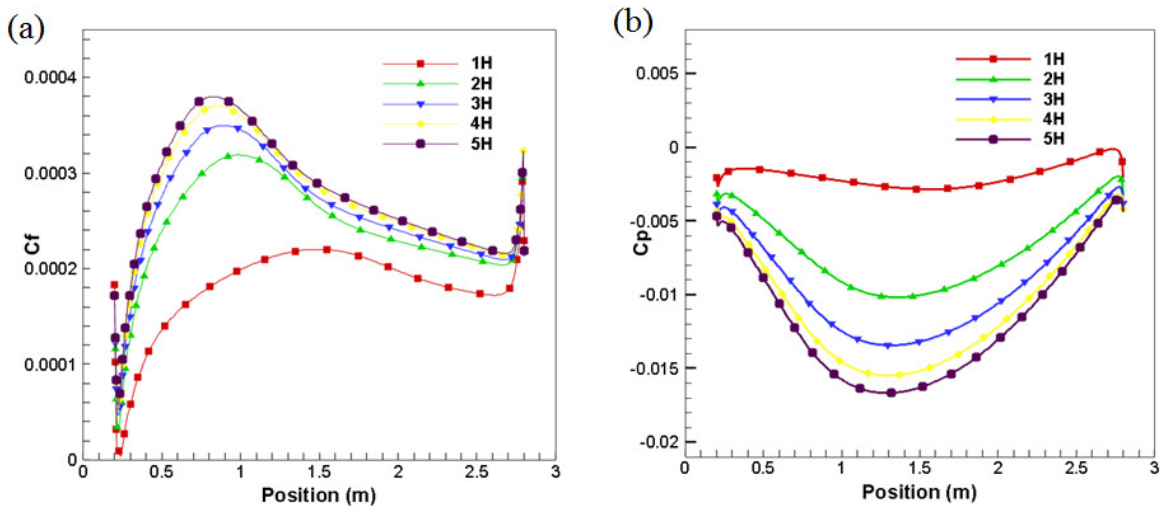

Figure 6: Coefficient of (a) frictionC_f and (b) pressureC_p, at the hot wall according sunshine.

3.4. Field temperature

The field simulated temperatures simulated inside were plotted in Figure 7. Note also that the injected air is warmer. The temperature at the ceiling of the enclosure is greater. The heat distribution appears more uniform, and more laminated. This result confirms the observations made by [26-27-28]. Colder areas are observedeven at the bottom of the enclosure which enters through the bottom opening.

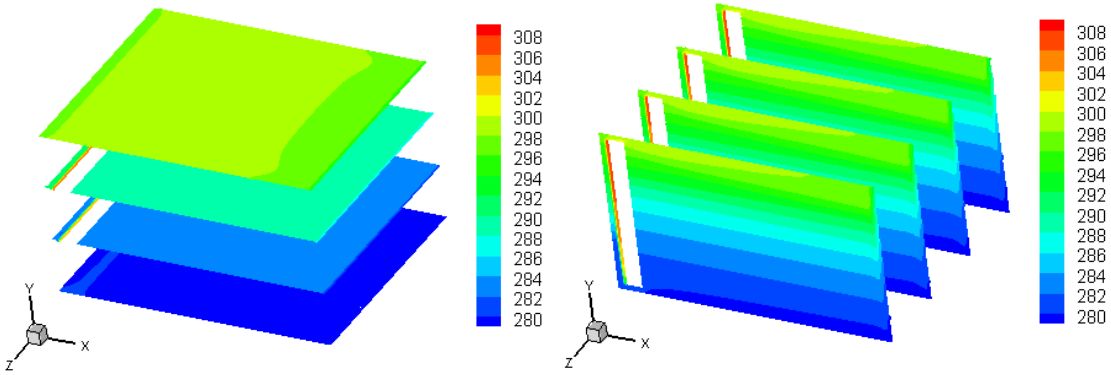

Figure 7: Average temperature field.

3.5. Analysis of the Flow Pattern in the Air Channel

The results (Figure 8) show that the transition on massive wall side mostly occurs at the height between 0.6m and 0.8m. When the natural convection is relatively weak, the transition occurs at the height between 0.8m and 1m. The airflow of both sides at least half height is turbulent. The airflow in the channel isn't always laminar or turbulent and is a complex flow, with the transition from laminar to turbulent.

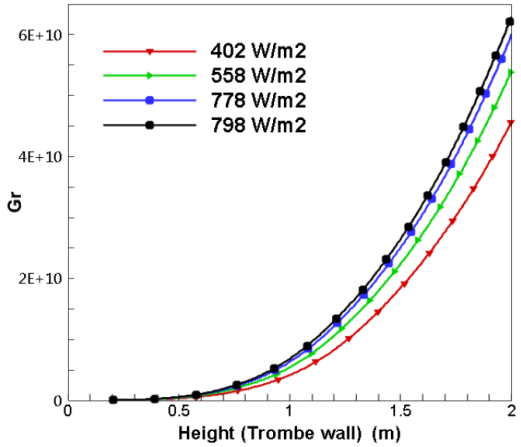

Figure 8: The number of local Grashof along the Trombe wall.

The exchange of the flow characteristics along the Trombe wall (h,Gr_h), we see that the flow is laminar in the area (h < 0.67 m, Gr_h< $4x10^8$), in the transitionalarea (0.67m < h < 0.8 m, $4x10^8$<Gr_h< 10^9), and turbulence in the area (h > 0.8 m,Gr_h>10^9).

3.6. Velocity at the openings

Figure 9. Represents the evolution of the speed to high and low openings settings, we notice a profile of velocity under parabolic shape openings to low levels due to the channel effect (suction area of cold air), and detachment at the levels of top openings (outlet area of the hot air) due to the detachment of the hot boundary layer.

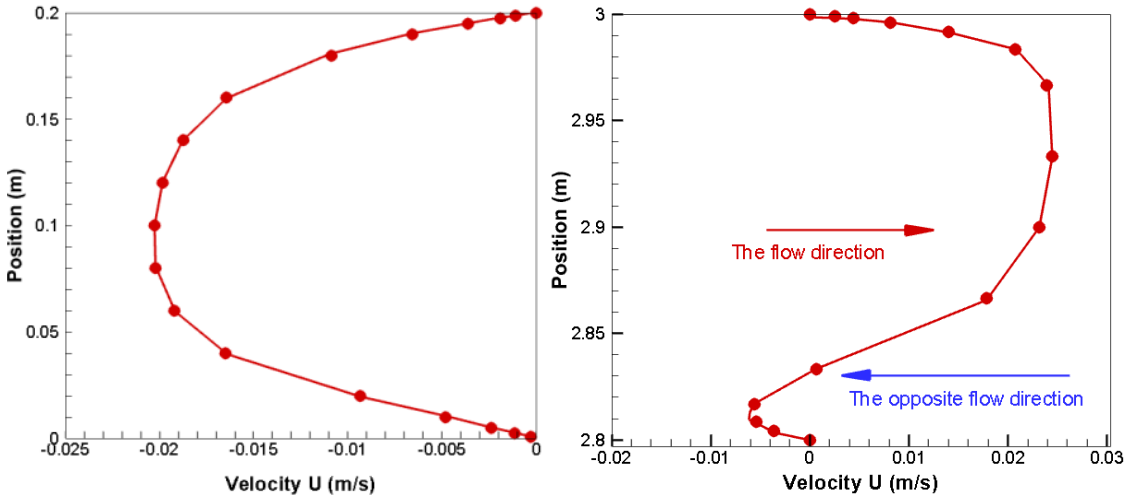

Figure 9: Velocity at the openings a) low and b) high.

The viscosity slows in particular flow near the wall. The positive pressure gradient helps to slow down the flow, slowing up to the cancellation of the velocity near the wall and its inversion is the case of separation of the boundary layer observed at the high opening, Figure 9.

The Figure 10. shows the velocity contours in the direction of flow levels in the median planes (X, Y and Z) where it is clear that the flow is greatly accelerated in the hot zone and the cold zone. It is obvious that the

upper and lower openings through its presence's in the channel reduce the flow area causing a strong acceleration of the flow.

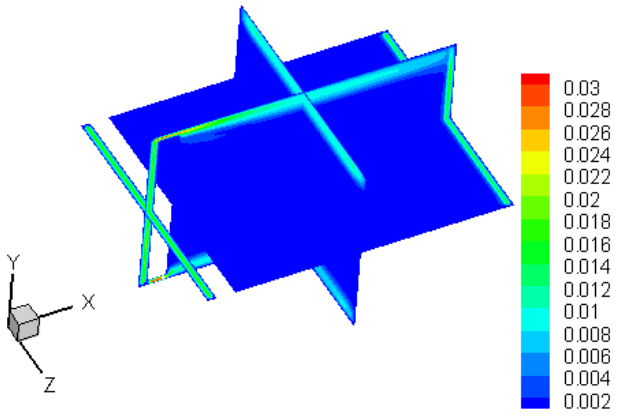

Figure 10: Velocity level median planes (X, Y and Z).

3.7. Velocity and temperature near the hot and cold walls

This section is to describe the changes in the different velocity profiles and temperature, depending on the height of the hot and cold wall.

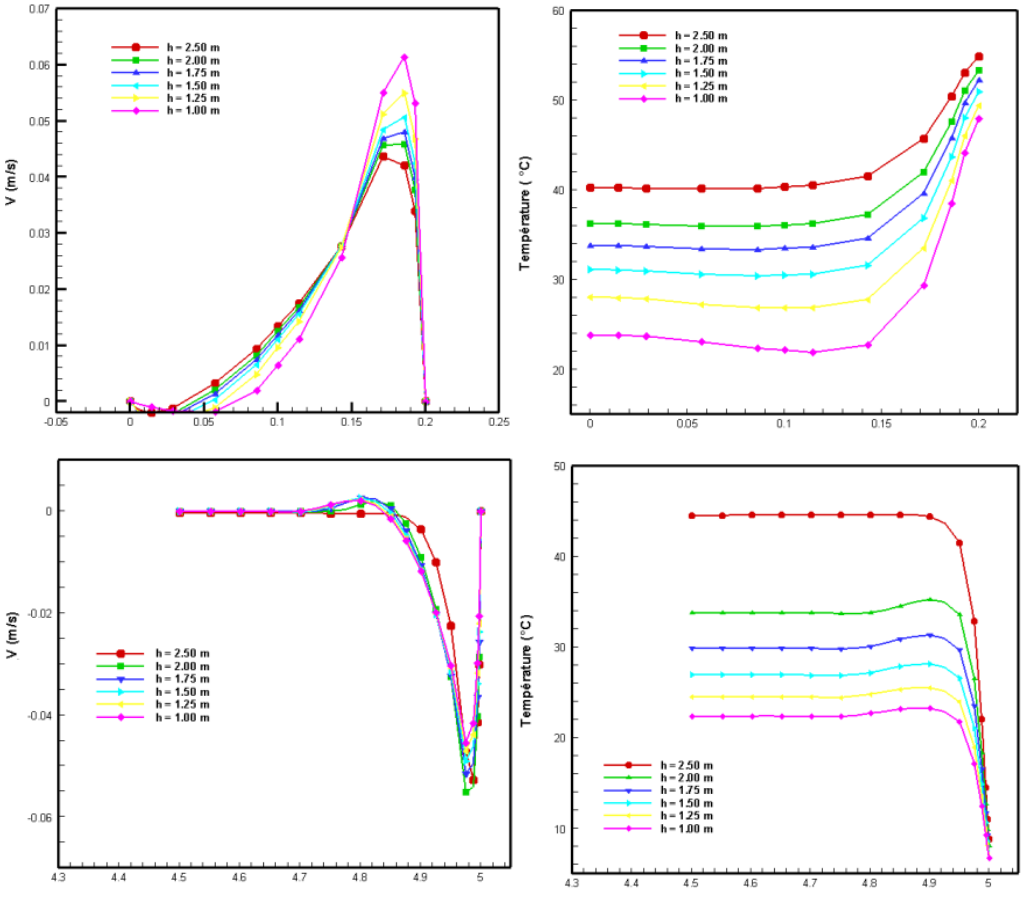

Figure 11: Profile of the Velocity and the Temperature, close to the wall: a) hot and b) cold, depending on the height h.

Developments different profiles velocitys and temperatures, depending on the sunlight hours in, it is based on the numerical results, during which the simulations were made near the hot and cold wall. The study of flow approximately the walls Figure11. is necessary for the determination of heat transfer by convection between the wall and the air around it. Away from the hot surface, air at an average speed V_m and an average temperature

T_m. In the immediate vicinity of the surface, the air temperature is very close to that of the surface. The air velocity is almost zero.

3.8. Effect (3D) of the flow

The fields in the turbulent intensity and turbulent kinetic energy are shown in Figure 11. As output, we see that the flow is almost up, and is symmetrical with respect to the center enclosure. The minimum slightly shift the left and right side of the room, creating a slight asymmetry of the profiles. There is a slight 3D effect on the profiles of 1/4 shots (left) and 4/4 (right) side of the upper opening of the enclosure. This seems due to the interaction between the plume and the fresh air that enters the enclosure through the lower opening. In this case, the plans, profiles1/4 and 4/4 are deformed from the plane in the center of the room.

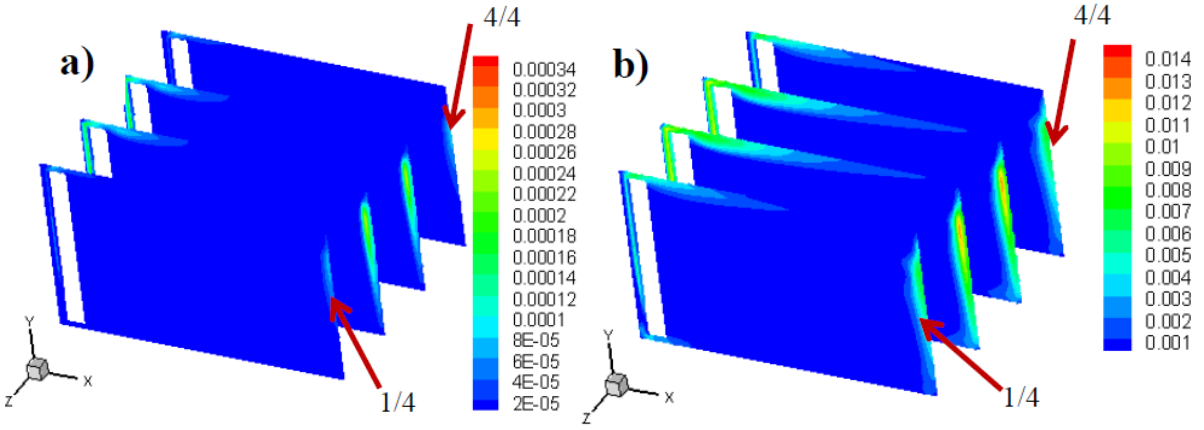

Figure 12:. Effect 3D in the flow, a) turbulent kinetic energy, b) turbulent intensity

Is at the upper opening and the hot and cold walls the velocity profiles differ most and 3D effects are most visible in Figure 12. The speeds pass through a maximum at the top of the opening higher. Negative velocities characterizing a fresh air inlet through the lower opening, the speeds are negative in the majority in the basic opening and positive in the high opening. This means there is simultaneously a cool flow of air that enters the enclosure from the bottom and a flow of hot air coming from the top, so it is the case of passive heating by thermal-circulation.

Conclusion

The simulation results shown in this work, they allow the presentation and exploitation of results obtained from simulations in 3D. They were made with a heating, condition due to sunlight by numbers of modified Grashof (Gr_h) between 10^7 and 10^{11}. All the thermal, dynamics and turbulence parameters are calculated according to the climate conditions of the area studied.

The natural convection in the channel is fairly complex; it changes from the laminar flow to the turbulent flow and the turbulent flow covers at least half the height of massive wall during the normal circulation. The velocity profiles and the average temperature were presented and analyses. The study of these profiles based on the height in the channel has helped identify a flow regime change. This change in diet is characterized by increased convective transfer. Three zones have been defined along the hot wall (Trombe wall): a laminar, transitional and turbulent zone.

The near wall region serves as a motor to flow, substantially all of the injected energy to the thermal wall remains confined in this region and serves to accelerate the fluid. The neutral zone (laminating zone), is driven by the near wall region and decelerated with the height retention rate. The flow prior the transition is a shearing flow, the velocity fluctuations are increases with shearing in the channel.

Competition settles then between the heating walls which tends to increase shearing and turbulent mixing, created by shearing, which tends to equalize the flow and reducing the shearing. When this turbulent mixture becomes significant enough, a flow regime change occurs, it is the mixing zone. In this zone, located after the transition, the flow is mixed, homogenized by turbulent mixing; shearing decreases and the channel center is warming. Velocity fluctuations are no longer fed by the shearing, but directly from the turbulent flow of heat. Indeed, an analysis of the terms of production of turbulent kinetic energy shows a competition between theviscous origin production, which dominates in channel input and that of thermal origin which grows before the transition and after dominates. This behaviour analysis allows us to offer an explanation of the shape of the behaviour curves Figure 3, giving the **Nusselt** number (Nu) based on the **Grashof** (**Grh**) along the canal.

Nomenclature

D	diffusion coefficient [$m^2 .s^{-1}$]
D^*	diffuse solar flux [W/m²]
S^*	direct solar flux [W/m²]
e	wall thickness [m]
f_i	body forces [kg.m s^{-2}]
I	local depth [m]
J	width of the room studied [m]
k	turbulent kinetic energy [$m^2 .s^{-2}$]
p	pressure [Pa]
P'_i	pressure fluctuation [Pa]
H	room height [m]
h	height Trombe wall [m]
h_i	height of the lower opening [m]
h_o	height of the top opening [m]
h_c	convective exchange coefficient [W/m.K]
t	time [s]
T_{ex}	outside temperature [°C]
T_{in}	inside temperature [°C]
T_{moy}	average temperature [°C]
u_i	velocity component [$m.s^{-1}$]
u'_i	fluctuation of the velocity
u^+	velocity of the boundary layer
u_τ	velocity characteristic of friction
y^+	wall distance : $y^+ = yu_\tau / v$
α_t	turbulent thermal diffusivity [$m^2.s^{-1}$]
λ	thermal conductivity [W/m.K]
ρ	density [kg/m^3]
β	volumetric expansion [K^{-1}]
δ	thickness of the air gap [m]
δ_{ij}	the Kronecker symbol
ε	dissipation rate [$m^2 .s^{-2}$]
φ_s	heat flux due to insolation [W/m²]
τ_w	Constraint Ranking
μ	dynamic viscosity [$m^2 .s^{-2}$]
v	kinematic viscosity [$m^2 .s^{-2}$]

Exhibitor, Index

in	inside
ex	outside
s	solar
o	high
b	low
w	wall
f	fluid

Références

[1] J. N. MitogoEseng, “Quantification expérimentale des performances d’undispositif de bardage avec lame d’air tampon et parement en bois,” Thèse de doctorat, Université Bordeaux, p. 126, 2012.
[2] W. Aung, L. Fletcher, and V. Sernas, “Developing laminar free convection between vertical flat plates with asymmetric heating,” Heat Mass Transfer 15, 2293–2308, 1972.
[3] A. Kaiser, B. Zamora, and A. Viedma, “Correlation for Nusselt number in natural convection in vertical convergent channels at uniform wall temperature by a numerical investigation,” Heat Fluid Flow 25(4), 671–682, 2004.
[4] G. Gan, “A parametric study of Trombe walls for passive cooling of buildings,” Energy Build.27, 37, 1998.
[5] G. Gan, “Simulation of buoyancy-induced flow in open cavities for natural ventilation,” Energy Build.38(5), 410–420, 2006.
[6] S. A. M. Burek and A. Habeb, “Air flow and thermal efficiency characteristics in solar chimneys and Trombe walls,” Energy Build. 39, 128–135, 2007.
[7] K. S. Ong, “A mathematical model of a solar chimney,” Renewable Energy 28, 1047–1060, 2003.
[8] C. Balocco, “A simply model to study ventilated façades energy performance,” Energy Build. 34, 469–475, 2002.
[9] A. Bouchair, “Solar chimney for promoting cooling ventilation in southern Algeria,” Build. Serv. Eng. Res. Technol. 15(2), 81–93 (1994).
[10] N. K. Bansal, M. Jyotirmay, M. Sanjay, and J. Meenakshi, “Modeling of window sized solar chimneys for ventilation”, Build. Environ. 40, 1302–1308, 2005.
[11] N. Chami and A. Zoughaib, “Modeling natural convection in a pitched thermo-syphon system in building roofs and experimental validation using particle image velocimetry,” Energy Build. 42(8), 1267–1274, 2010.
[12] K. Hami, B. Draoui, and L. Belloufa, “Modeling of a Heating Passive System”, International Review of Mechanical Engineering, 4(4), 376-380, 2010.

[13] B. Zamora and A. S. Kaiser, “Optimum wall-to-wall spacing in solar chimney shaped channels in natural convection by numerical investigation,” Appl. Therm. Eng. 29(4), 762–769, 2009.
[14] G. Gan, “General expressions for the calculation of air flow and heat transfer rates in tall ventilation cavities,” Build. Environ. 46(10), 2069–2080 (2011).
[15] K. Hami, B. Draoui, and O. Hami, “The thermal performances of a solar wall,” Energy 39, 11–16 (2012).

[16] P. Chassaing, Turbulence en mécanique des fluide: Analyse du phénomène en vue de sa modélisation à l'usage de l'ingénieur,Polytech (Cepadues, 2000).
[17] R. Schiestel, Les écoulements turbulents: Modélisation et simulation , 2nd ed. (Hermes, 1998).
[18] A. Fourar, O. Timizar, and F. Abdessemed, "Contribution à l'etude d'un écoulement turbulent dans une conduite. Développement de la couche limite turbulente," ScienceLib Editions Mersenne (2011), Vol. 3, No. 110302, ISSN 2111- 4706; avalable at http://www.sciencelib.fr/IMG//pdf/OMAR2.pdf.
[19] S. V. Patankar, Numerical Heat Transfer and Fluid Flow (Hemisphe`re Inc., McGraw-Hill, Washington, Etats-Unis, 1980), pp. 197.
[20] K. Abe, N. Higashimori, M. Kubo, and Y. Iso, "A remark on the Courant-Friedrichs-Lewy Condition in finite difference approach to PDE's," Adv. Appl. Mathematics Mechanics 6(5), 693–698 (2014).
[21] L. T. Wong and W. K. Chow, "Solar radiation model," Appl. Energy 69, 191–224 (2001).
[22] N. Marzouqy and T. P. Fluent, Cours Mécanique des Fluides (Université des Mines, Paris, 2006), p. 31.
[23] C. Bin, Z. Jinling, C. Cuiying, and Z. Zhi, "Experimental Investigation of Natural Convection in Trombe Wall Systems," in Envelope Technologies for Building Energy Efficiency, ICEBO2006, Shenzhen, China, 2006.
[24] A. Trombe et al., "Use of inverse method of determine natural convection heat transfer coefficients in unsteady state," J. Heat Transfer 125, 1017–1026 (2003).
[25] J. Salat, S. Xin, P. Joubert, A. Sergent, F. Penot, and P. Le Quere, "Experimental and numerical investigation of turbulent natural convection in a large air-filled cavity," Heat Fluid Flow 25, 824–832 (2004).
[26] S. Peng and L. Davidson, "Large eddy simulation for turbulent buoyant flow in a confined cavity," Heat Fluid Flow 22, 323–331 (2001).
[27] A. Sergent, P. Joubert, and P. Le Quere, "Development of a local subgrid diffusivity model for large eddy simulation of buoyancy driven flows: Application to a square differentially heated cavity," Numer. Heat Transfer 44(8), 789–810 (2003).